



# Forced convection gaseous slip flow in a porous circular microtube: An exact solution



Keyong Wang <sup>a, b</sup>, Fatmeh Tavakkoli <sup>b</sup>, Shujuan Wang <sup>b</sup>, Kambiz Vafai <sup>b, \*</sup>

<sup>a</sup> School of Mechanical Engineering, Shanghai University of Engineering Science, Shanghai 201620, China

<sup>b</sup> Department of Mechanical Engineering, University of California, Riverside, CA 92521, USA

## ARTICLE INFO

### Article history:

Received 23 February 2015

Received in revised form

10 June 2015

Accepted 13 June 2015

Available online 21 July 2015

### Keywords:

Porous medium

Forced convective heat transfer

Local thermal non-equilibrium

Microtube

Rarefaction effect

## ABSTRACT

Rarefied phenomena can occur when a gas flows through a microchannel. However, most available convective solutions were obtained under the local thermal equilibrium condition. In this study, gaseous slip flow in a circular microtube filled with a porous medium is analytically investigated under the local thermal non-equilibrium condition. The first-order velocity slip and temperature jump conditions at the tube wall are invoked in order to account for the rarefaction effects. Rigorous analytical solutions are obtained for the velocity and temperature distributions as well as the average Nusselt number. Theoretical predictions are then compared to those of existing limiting cases in the literature. Results indicate that the degree of rarefaction, represented by the Knudsen number ranging from  $10^{-3}$  to  $10^{-1}$ , has a significant effect on the velocity, temperature, pressure drop and heat transport within the microtube for various combinations of pertinent parameters such as the porosity, effective thermal conductivity ratio, Biot number and porous media shape factor.

© 2015 Elsevier Masson SAS. All rights reserved.

## 1. Introduction

Due to the miniaturization of electronics and advances in micro-fabrication, the research on gas transport phenomena at micro scale is receiving growing attention. And investigators have found new applications such as smaller flow passages and fins employed in compact heat exchangers and electronics cooling in the emerging field of micro-scale heat transfer. The gas flow in a microchannel is associated with the so-called rarefaction effect, which is measured by the Knudsen number ( $Kn$ ) defined as the ratio of the molecular mean free path ( $\lambda$ ) to the appropriate characteristic dimension of the flow domain. Typical applications in microfluidic systems may involve characteristic dimensions in the range of 10–200  $\mu\text{m}$  [1]. According to the degree of rarefaction effect, there are four models including the continuum regime ( $Kn \leq 10^{-3}$ ), slip-flow regime ( $10^{-3} < Kn \leq 10^{-1}$ ), transition regime ( $10^{-1} < Kn \leq 10$ ) and free molecular regime ( $Kn > 10$ ). In the slip-flow regime, the deviation from the continuum behavior is very slight, corresponding to Knudsen numbers in the range of  $10^{-3}$  to  $10^{-1}$  [2–4]. Therefore, the standard Navier–Stokes and energy

equations can still be employed with the proper boundary conditions accounting for velocity-slip and temperature-jump at the walls [1,4].

The slip-flow and heat transfer in various-shaped micro-channels have been investigated in the past decades. However, forced convective heat transfer within porous microchannels has not been studied extensively subject to the rarefied condition [5]. One of the earliest contributions on forced convection with the slip-flow in a porous parallel-plate microchannel or circular microtube was investigated analytically by Nield and Kuznetsov [6]. According to their findings, the velocity slip results in heat transfer enhancement and temperature jump leads to a reduction in heat transfer. Subsequently, Kuznetsov and Nield [7] extended their work to the case of thermally developing forced convection. Had-dad et al. [8] numerically studied the laminar forced convection of gaseous slip flow in a porous circular microtube. Hooman [9] dealt with the slip flow in a porous rectangular microchannel. Closed form solutions for fully developed velocity and temperature distributions were obtained using a Fourier series approach. Shoukouhmand et al. [10] carried out numerical simulation of Darcy–Brinkman–Forchheimer flow model and forced convection in a circular micro- and nanotube filled with a porous medium by invoking the velocity slip and temperature jump conditions. They found that the variations of Knudsen number exhibit considerable

\* Corresponding author.

E-mail address: [vafai@engr.ucr.edu](mailto:vafai@engr.ucr.edu) (K. Vafai).

Nomenclature		$\hat{u}$	dimensionless velocity
$a_{sf}$	interfacial area per unit volume of the porous medium ( $m^{-1}$ )	$z$	axial coordinate
$Bi$	Biot number, $h_{sf}a_{sf}R^2/k_{s,eff}$	<i>Greek symbols</i>	
$c_p$	specific heat of the fluid ( $J\ kg^{-1}\ ^\circ C^{-1}$ )	$\gamma$	specific heat transfer ratio
$Da$	Darcy number	$\delta$	$\sqrt{Bi(1+\kappa)/\kappa}$
$f$	Fanning friction factor	$\varepsilon$	porosity
$h_{sf}$	interstitial heat transfer coefficient ( $W\ m^{-2}\ ^\circ C^{-1}$ )	$\eta$	dimensionless radial coordinate, $r/R$
$k_f$	thermal conductivity of the fluid ( $W\ m^{-1}\ ^\circ C^{-1}$ )	$\theta$	dimensionless temperature, $k_{s,eff}(T - T_w)/q_w R$
$k_{f,eff}$	effective thermal conductivity of the fluid ( $W\ m^{-1}\ ^\circ C^{-1}$ )	$\kappa$	ratio of the effective thermal conductivity of the fluid to that of the solid, $k_{f,eff}/k_{s,eff}$
$k_s$	thermal conductivity of the solid ( $W\ m^{-1}\ ^\circ C^{-1}$ )	$\lambda$	molecular mean free path (m)
$k_{s,eff}$	effective thermal conductivity of the solid ( $W\ m^{-1}\ ^\circ C^{-1}$ )	$\mu$	dynamic viscosity (Pa s)
$K$	permeability ( $m^2$ )	$\rho$	density of the fluid ( $kg/m^3$ )
$Kn$	Knudsen number	$\sigma_t$	thermal accommodation coefficient
$M$	ratio of the actual to effective viscosity of the fluid, $\mu_{eff}/\mu_f$	$\sigma_v$	tangential momentum accommodation coefficient
$Nu$	average Nusselt number at the wall for LTNE model	$\varphi_t$	temperature jump coefficient, $[(2 - \sigma_t)/\sigma_t][2\gamma/(\gamma + 1)]Kn/Pr$
$Nu_1$	average Nusselt number at the wall for LTE model	$\varphi_v$	velocity slip coefficient, $[(2 - \sigma_v)/\sigma_v]Kn$
$p$	pressure (Pa)	$\omega$	porous media shape factor, $1/\sqrt{MDa}$
$P$	dimensionless pressure gradient	<i>Subscripts/superscripts</i>	
$Pr$	Prandtl number of the fluid	e	entrance
$q_w$	imposed heat flux on the wall ( $W/m^2$ )	eff	effective
$r$	radial coordinate	f	fluid phase
$R$	radius of the microtube (m)	m	mean value
$Re$	Reynolds number	s	solid phase
$T$	temperature ( $^\circ C$ )	w	tube wall subject to a constant heat flux
$u$	fluid velocity (m/s)		

effects on heat transfer and temperature distribution across the cross section of the tube. Hashemi et al. [11] analytically investigated forced convective heat transfer in a porous microannulus for two distinct thermal boundary conditions, and found that the Nusselt number decreases as the Knudsen number or annulus aspect ratio increases. Other contributions to the slip flow in porous media were made by Haddad and co-workers [12], Hooman [13] and Chauhan and Kumar [14]. All the above contributions were based on the local thermal equilibrium (LTE) model, which ignores the temperature difference between the fluid and solid phases.

When the heat exchange between the two phases is not sufficiently strong, the LTE assumption breaks down [15]. In such situations, the local thermal non-equilibrium (LTNE) model should be utilized for analyzing the rarefaction effects on the velocity and temperature distributions. Haddad et al. [16] numerically investigated the hydrodynamically fully developed and thermally developing forced convection of the gaseous slip flow in a porous parallel-plate microchannel or circular microtube with constant wall temperature. In their simulations, it is found that the heat transfer decreases with an increase in the Knudsen number or Forchheimer number and increases with an increase in the Péclet number or Darcy number. Most recently, Buonomo et al. [5] analytically studied the rarefied gaseous slip flow in a porous parallel-plate microchannel. The exact solutions for the fluid and solid temperatures were derived under LTNE and constant heat flux conditions. Different trends were reported with respect to tangential momentum accommodation coefficient.

To the authors' knowledge, no attempt has been analytically or numerically made for evaluating the behavior of gaseous flow in porous circular microtubes under the LTNE condition. In the current

study, the rarefaction effect ( $10^{-3} < Kn \leq 10^{-1}$ ) is therefore analytically treated with respect to the first-order slip/jump conditions. Exact solutions for the velocity, fluid and solid temperature distributions and the average Nusselt number are derived. The effects of various thermophysical properties on the heat transfer within the porous circular microtube are also studied.

## 2. Mathematical model and analysis

### 2.1. Governing equations

A schematic view of a circular microtube filled with a porous medium and the cylindrical coordinate system ( $r, z$ ) is depicted in Fig. 1. The radius is  $R$  and a constant heat flux  $q_w$  is uniformly imposed on the impermeable tube wall. The flow direction of the rarefied gas is along the  $z$ -axis. The following assumptions are invoked in the present study:

- The flow is steady and incompressible and Brinkman-extended Darcy model is considered.
- Natural convection, dispersion and radiative heat transfer are negligible.
- Axial heat conduction is assumed to be negligible.
- The flow is hydrodynamically and thermally fully developed with temperature independent properties.

Under the foregoing assumptions the Brinkman momentum and energy equations using the local thermal non-equilibrium condition in cylindrical coordinates are expressed as [17,18].

Brinkman momentum

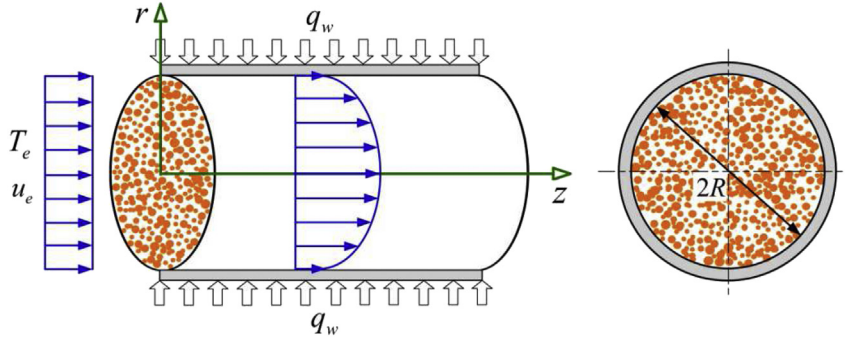


Fig. 1. Schematic diagram of a circular microtube filled with a porous medium.

$$\mu_{\text{eff}} \left( \frac{d^2 u}{dr^2} + \frac{1}{r} \frac{du}{dr} \right) - \frac{\mu_f}{K} u - \frac{dp}{dz} = 0 \quad (1)$$

Fluid phase energy

$$k_{f,\text{eff}} \frac{1}{r} \frac{\partial}{\partial r} \left( r \frac{\partial T_f}{\partial r} \right) + h_{\text{sf}} a_{\text{sf}} (T_s - T_f) = \rho c_p u \frac{\partial T_f}{\partial z} \quad (2)$$

Solid phase energy

$$k_{s,\text{eff}} \frac{1}{r} \frac{\partial}{\partial r} \left( r \frac{\partial T_s}{\partial r} \right) - h_{\text{sf}} a_{\text{sf}} (T_s - T_f) = 0 \quad (3)$$

where

$$\mu_{\text{eff}} = \frac{\mu_f}{\varepsilon}, \quad k_{f,\text{eff}} = \varepsilon k_f, \quad k_{s,\text{eff}} = (1 - \varepsilon) k_s \quad (4)$$

here  $u$  is the fluid velocity,  $\mu_{\text{eff}}$  an effective viscosity,  $\mu_f$  the dynamic viscosity of the fluid,  $K$  the permeability of the porous medium,  $p$  the applied pressure and  $T_f$ ,  $T_s$ ,  $k_{f,\text{eff}}$ ,  $k_{s,\text{eff}}$ ,  $\varepsilon$ ,  $\rho$  and  $c_p$  the fluid and solid temperatures, the effective thermal conductivities, porosity, the density and specific heat of the fluid respectively. The coupling between the two energy equations is achieved using the fluid–solid interfacial term which represents the heat transfer between the two phases via the heat transfer coefficient  $h_{\text{fs}}$  and the specific surface area  $a_{\text{fs}}$ .

To consider the effects of flow rarefactions at the tube wall, the first-order velocity slip boundary condition is prescribed by Refs. [10,19]

$$u_{f,w} - u_w = -\alpha_v \lambda \left( \frac{\partial u}{\partial r} \right)_{r=R}, \quad \alpha_v = \frac{2 - \sigma_v}{\sigma_v} \quad (5)$$

where  $u_{f,w}$  denotes the fluid velocity immediately adjacent to the tube wall,  $u_w$  the wall velocity,  $\alpha_v$  the momentum slip factor and  $\sigma_v$  the tangential momentum accommodation coefficient. It should be noted that  $u_w = 0$  for the stationary wall. The axisymmetry at the center,  $r = 0$ , for the fluid velocity is given by

$$\left. \frac{du}{dr} \right|_{r=0} = 0 \quad (6)$$

Similarly, the gas temperature at the tube wall differs from the wall temperature in proportion to the local normal temperature gradient. The corresponding temperature-jump boundary condition reads [10,19]

$$T_{f,w} - T_w = -\alpha_t \lambda \left. \frac{\partial T_f}{\partial r} \right|_{r=R}, \quad \alpha_t = \frac{2 - \sigma_t}{\sigma_t} \frac{2\gamma}{\gamma + 1} \frac{1}{Pr} \quad (7)$$

where  $T_{f,w}$  denotes the fluid temperature immediately adjacent to the tube wall,  $T_w$  the wall temperature which is not known *a priori* and must be obtained as part of the solution,  $\alpha_t$  the temperature jump factor,  $\sigma_t$  thermal accommodation coefficient,  $\gamma$  the specific heat ratio and  $Pr$  the Prandtl number. From the physical point of view, the values of  $\sigma_v$  and  $\sigma_t$  vary from unity (complete accommodation, diffuse reflection) to zero (specular reflection) [20]. Generally,  $\sigma_v$  and  $\sigma_t$ , which are both dependent on the surface finish, the fluid temperature and pressure, need to be determined experimentally. Among most investigations  $\sigma_v$  and  $\sigma_t$  are assumed to be equal to 1. However, experimental measurements illustrated that both values are less than unity [4]. Therefore, as suggested by Bahrami et al. [4] and Cai et al. [21], both  $\sigma_v$  and  $\sigma_t$  are assumed to be 0.85 in the present study unless otherwise stated. Thermal creep and viscous dissipation have been neglected in Eqs. (5) and (7) as explained by Kennard [19].

The imposed heat flux  $q_w$  can be divided between the fluid and solid phases depending on their effective conductivities and corresponding temperature gradients at the tube wall. That is [18,22]

$$q_w = k_{f,\text{eff}} \left. \frac{\partial T_f}{\partial r} \right|_{r=R} + k_{s,\text{eff}} \left. \frac{\partial T_s}{\partial r} \right|_{r=R} \quad (8)$$

As addressed by Lee and Vafai [23], the temperatures of the fluid and solid phases at the wall will be the same when a tube with finite thickness wall and high thermal conductivity is attached to a porous medium. Consequently,

$$T_f|_{r=R} = T_s|_{r=R} \quad (9)$$

The axisymmetry at the center,  $r = 0$ , leads to the thermal boundary condition as follows

$$\left. \frac{\partial T_f}{\partial r} \right|_{r=0} = \left. \frac{\partial T_s}{\partial r} \right|_{r=0} = 0 \quad (10)$$

## 2.2. Hydrodynamic analysis

After employing the following dimensionless variables

$$\eta = \frac{r}{R}, \quad \tilde{u} = \frac{\mu u}{R^2 (-dp/dz)}, \quad M = \frac{\mu_{\text{eff}}}{\mu}, \quad Da = \frac{K}{R^2} \quad (11)$$

the Brinkman momentum Eq. (1) can be written in a dimensionless form

$$M \left( \frac{d^2 \tilde{u}}{d\eta^2} + \frac{1}{\eta} \frac{d\tilde{u}}{d\eta} \right) - \frac{\tilde{u}}{Da} + 1 = 0 \quad (12)$$

where  $M$  denotes the ratio of the actual to effective viscosity of the fluid and  $Da$  the Darcy number.

The dimensionless velocity slip and axisymmetric boundary conditions can be presented as

$$\tilde{u}(1) = -\varphi_v \left. \frac{d\tilde{u}}{d\eta} \right|_{\eta=1}, \quad \varphi_v = \alpha_v Kn \quad (13)$$

$$\left. \frac{d\tilde{u}}{d\eta} \right|_{\eta=0} = 0 \quad (14)$$

in which the Knudsen number is based on the hydraulic diameter as  $Kn = \lambda/R$ . As a result, Eq. (12) can be solved for the dimensionless velocity  $\tilde{u}$  subject to boundary conditions given by Eqs. (13) and (14) as

$$\tilde{u} = Da \left[ 1 - \frac{I_0(\omega\eta)}{\varphi_v \omega I_1(\omega) + I_0(\omega)} \right] \quad (15)$$

where  $I_\zeta$  is the  $\zeta$ th order modified Bessel function of the first kind and  $\omega = \sqrt{1/MDa}$  the porous media shape factor.

Introducing the dimensionless mean velocity  $\tilde{u}_m$  defined by

$$\tilde{u}_m = 2 \int_0^1 \tilde{u} \, d\eta \quad (16)$$

and then a further dimensionless form of  $\hat{u}$  is calculated as

$$\hat{u} = \frac{\tilde{u}}{\tilde{u}_m} = \frac{\omega[\psi I_0(\omega) - I_0(\omega\eta)]}{\psi \omega I_0(\omega) - 2I_1(\omega)} \quad (17)$$

where

$$\psi = 1 + \frac{\varphi_v \omega I_1(\omega)}{I_0(\omega)} \quad (18)$$

Having obtained the velocity field, we can proceed with the calculation of the Fanning friction factor as

$$f = \frac{2R \frac{dp}{dz}}{\frac{1}{2} \rho u_m^2} = \frac{8P}{DaRe} \quad (19)$$

where  $u_m$  is the mean velocity,  $Re$  the Reynolds number and  $P$  the dimensionless pressure gradient, which are respectively defined by

$$u_m = \frac{2}{R^2} \int_0^R ur \, dr, \quad Re = \frac{\rho u_m (2R)}{\mu_{eff}}, \quad P = -\frac{K}{\mu u_m} \frac{dP}{dz} \quad (20)$$

In a similar way as done by Lu et al. [24], the expression of  $P$  can be further given as

$$P = \frac{\psi \omega I_0(\omega)}{\psi \omega I_0(\omega) - 2I_1(\omega)} \quad (21)$$

Consequently, the dimensionless pressure drop, represented by  $fRe$ , reads

$$fRe = \frac{8}{\varepsilon} \frac{\psi \omega^3 I_0(\omega)}{\psi \omega I_0(\omega) - 2I_1(\omega)} \quad (22)$$

### 2.3. Heat transfer analysis

In this section, we shall seek exact solutions for forced convective heat transfer in a circular microtube filled with a porous medium under the local thermal non-equilibrium condition.

Adding the two energy equations (2) and (3), integrating with respect to  $r$  over the entire cross-sectional area and considering boundary conditions given by Eqs. (8) and (10) produce

$$\rho c_p u_m \frac{\partial T_{f,b}}{\partial z} = \frac{2q_w}{R} \quad (23)$$

in which  $\partial T_{f,b}/\partial z = \partial T_f/\partial z = \partial T_s/\partial z = \partial T_w/\partial z = \text{const}$  due to the assumption of fully developed flow.

Using the following dimensionless variables

$$\begin{aligned} \kappa &= \frac{k_{f,eff}}{k_{s,eff}}, \quad Bi = \frac{h_{sf} a_{sf} R^2}{k_{s,eff}}, \quad \theta_f = \frac{k_{s,eff}(T_f - T_w)}{q_w R}, \quad \theta_s \\ &= \frac{k_{s,eff}(T_s - T_w)}{q_w R} \end{aligned} \quad (24)$$

where  $\kappa$  is the ratio of the effective thermal conductivity of the fluid to that of the solid. Eqs. (2), (3), (7), (9) and (10) can be rewritten in the dimensionless form

$$\kappa \frac{1}{\eta} \frac{\partial}{\partial \eta} \left( \eta \frac{\partial \theta_f}{\partial \eta} \right) + Bi(\theta_s - \theta_f) = 2\hat{u} \quad (25)$$

$$\frac{1}{\eta} \frac{\partial}{\partial \eta} \left( \eta \frac{\partial \theta_s}{\partial \eta} \right) - Bi(\theta_s - \theta_f) = 0 \quad (26)$$

$$\theta_f \Big|_{\eta=1} = -\varphi_t \left. \frac{\partial \theta_f}{\partial \eta} \right|_{\eta=1}, \quad \varphi_t = \alpha_t Kn \quad (27)$$

$$\theta_f \Big|_{\eta=1} = \theta_s \Big|_{\eta=1} \quad (28)$$

$$\left. \frac{\partial \theta_f}{\partial \eta} \right|_{\eta=0} = \left. \frac{\partial \theta_s}{\partial \eta} \right|_{\eta=0} = 0 \quad (29)$$

The two dimensionless energy Eqs. (25) and (26) are added, and  $\hat{u}$  is substituted from Eq. (17) to yield the following Euler–Cauchy equation

$$\frac{1}{\eta} \frac{\partial}{\partial \eta} \left( \eta \frac{\partial}{\partial \eta} \right) (\kappa \theta_f + \theta_s) = \frac{2\omega[\psi I_0(\omega) - I_0(\omega\eta)]}{\psi \omega I_0(\omega) - 2I_1(\omega)} \quad (30)$$

The solution to Eq. (30) has the form of

$$\theta_s = C_1 I_0(\omega\eta) + C_2 \eta^2 + C_3 - \kappa \theta_f \quad (31)$$

where  $C_1$ ,  $C_2$  and  $C_3$  are constants but  $C_3$  needs to be determined later.

$$C_1 = \frac{-2}{\omega[\psi \omega I_0(\omega) - 2I_1(\omega)]} \quad (32)$$

$$C_2 = \frac{1}{2} \frac{\psi \omega I_0(\omega)}{\psi \omega I_0(\omega) - 2I_1(\omega)} \quad (33)$$

Substituting Eqs. (31) and (17) into Eq. (25) results in the following modified Bessel equation

$$\kappa \frac{1}{\eta} \frac{\partial}{\partial \eta} \left( \eta \frac{\partial \theta_f}{\partial \eta} \right) - \delta^2 \theta_f = \frac{1}{\kappa} \left[ C_1 (\omega^2 - Bi) I_0(\omega \eta) - Bi C_2 \eta^2 + (4C_2 - Bi C_3) \right] \quad (34)$$

where  $\delta = \sqrt{Bi(1+\kappa)/\kappa}$ . To this end, the dimensionless energy equations (25) and (26) are decoupled. Subsequently, the closed form solution of Eq. (34) subject to boundary conditions (27) and (28) yields the dimensionless temperature distribution of the fluid phase as

$$\theta_f = D_1 I_0(\delta \eta) + D_2 I_0(\omega \eta) + D_3 \eta^2 + D_4 + \frac{C_3}{1+\kappa} \quad (35)$$

where

$$C_3 = I_0(\omega) C_1 (1+\kappa) \varphi_t \delta \{ [I_0(\omega) + \varphi_t \omega I_1(\omega)] D_2 + (1+2\varphi_t) D_3 + D_4 \} \frac{I_1(\delta)}{I_0(\delta)} - \left[ 1 + \varphi_t \delta \frac{I_1(\delta)}{I_0(\delta)} \right] \{ I_0(\omega) C_1 + C_2 + (1+\kappa) \varphi_t [\omega I_1(\omega) D_2 + 2D_3] \} \quad (36)$$

$$D_1 = \frac{-C_1 + C_2 - (1+\kappa)(D_3 + D_4) + [C_1 - (1+\kappa)D_2] I_0(\omega)}{(1+\kappa) I_0(\delta)} \quad (37)$$

$$D_2 = \frac{C_1 \omega^2 - Bi}{\kappa \omega^2 - \delta^2} \quad (38)$$

$$D_3 = \frac{C_2}{1+\kappa} \quad (39)$$

$$D_4 = \frac{4}{\delta^2} \left( D_3 - \frac{Bi}{4\kappa} - \frac{C_2}{\kappa} \right) \quad (40)$$

The tube wall heat transfer coefficient for the local thermal non-equilibrium model is obtained from

$$h_w = \frac{q_w}{T_w - T_{f,b}} \quad (41)$$

From the analytical solutions for the velocity and temperature distributions, the average Nusselt number on the tube wall is determined based on the overall thermal equivalent conductivity,  $k_{eq} = k_{f,eff} + k_{s,eff}$ , as

$$Nu = \frac{2Rh_w}{k_{eq}} = -\frac{2Rq_w}{k_{eq}(T_w - T_{f,b})} = -\frac{2k_{s,eff}}{k_{eq}\theta_{f,b}} = -\frac{2}{(1+\kappa)\theta_{f,b}} \quad (42)$$

Using Eqs. (17) and (35), the dimensionless bulk mean fluid temperature  $\theta_{f,b}$  can be obtained by averaging over the cross section of the tube

$$\begin{aligned} \theta_{f,b} &= 2 \int_0^1 \hat{u} \theta_f \eta d\eta \\ &= D_1 g_1 \frac{2}{\delta^2 - \omega^2} [\omega I_0(\omega) I_1(\delta) - \delta I_0(\delta) I_1(\omega)] + D_2 g_1 [I_0^2(\omega) - I_1^2(\omega)] \\ &\quad + D_3 g_1 \frac{2}{\omega^2} \left[ \left( \omega + \frac{4}{\omega} \right) I_1(\omega) - 2I_0(\omega) \right] + \left[ \left( D_4 + \frac{C_3}{1+\kappa} \right) g_1 \right. \\ &\quad \left. + D_2 g_2 \right] \frac{2}{\omega} I_1(\omega) + D_1 g_2 \frac{2}{\delta} I_1(\delta) + \frac{1}{2} \left[ D_3 + 2 \left( D_4 + \frac{C_3}{1+\kappa} \right) \right] g_2 \end{aligned} \quad (43)$$

where

$$g_1 = \frac{-\omega}{\psi \omega I_0(\omega) - 2I_1(\omega)} \quad (44)$$

$$g_2 = \frac{\psi \omega I_0(\omega)}{\psi \omega I_0(\omega) - 2I_1(\omega)} \quad (45)$$

It should be noted that the dimensionless bulk mean temperature  $\theta_{f,b}$  given by Eq. (43) is constant along the length of the tube. Using Eq. (24),  $\theta_{f,b}$  can be rewritten in another form as follows

$$\theta_{f,b} = \frac{k_{s,eff} (T_{f,b} - T_w)}{q_w R} \quad (46)$$

The temperature difference between the wall and the bulk fluid can be written as

$$T_w - T_{f,b} = -\frac{q_w R}{k_{s,eff}} \theta_{f,b} \quad (47)$$

where  $T_{f,b}$  is the bulk mean temperature that is defined by

$$T_{f,b} = \frac{2}{R^2 u_m} \int_0^R u T_f r dr \quad (48)$$

As highlighted by Mahjoob and Vafai [25], although the fluid temperature  $T_f$  in the fully developed region is a function of both transverse and longitudinal coordinates, the dimensionless fluid temperature  $\theta_f$  is a function of the transverse coordinate only and the dimensionless bulk mean temperature  $T_{f,b}$  is a function of the longitudinal coordinate only. Integrating both sides of Eq. (23) with respect to  $z$  and rearranging the resultant integration lead to

$$T_{f,b} = \frac{2q_w}{R\rho c_p u_m} z + T_e \quad (49)$$

Using the continuum equation, one can readily obtain the relationship  $u_m = u_e/\varepsilon$ . Thus, Eq. (49) can be rewritten as

$$T_{f,b} = \frac{2q_w \varepsilon}{R\rho c_p u_e} z + T_e \quad (50)$$

Substituting Eq. (50) into Eq. (47) results in the wall temperature

$$T_w = \frac{2q_w \varepsilon}{R\rho c_p u_e} z - \frac{q_w R}{k_{s,eff}} \theta_{f,b} + T_e \quad (51)$$

### 3. One equation model

Taking the limit of  $Bi \rightarrow \infty$ , the solution of the LTNE model reduces to that of the LTE counterpart. Herein, an alternative approach for the solution of the LTE model, namely one equation model, is addressed. The single energy equation for one equation model can be obtained by adding Eqs. (25) and (26), i.e. assuming that the fluid and solid temperatures are equal:  $\theta_f = \theta_s = \theta$

$$(1 + \kappa) \frac{1}{\eta} \frac{\partial}{\partial \eta} \left( \eta \frac{\partial \theta}{\partial \eta} \right) = \frac{2\omega[\psi I_0(\omega) - I_0(\omega\eta)]}{\psi \omega I_0(\omega) - 2I_1(\omega)} \quad (52)$$

The corresponding boundary conditions given by Eqs. (27)–(29) are simplified as

$$\theta|_{\eta=1} = -\varphi_t \frac{\partial \theta}{\partial \eta} \Big|_{\eta=1} \quad (53)$$

$$\frac{\partial \theta}{\partial \eta} \Big|_{\eta=0} = 0 \quad (54)$$

Therefore, the dimensionless temperature distribution for the one equation model takes the form of

$$\theta = E_1 I_0(\omega\eta) + E_2 \eta^2 + E_3 \quad (55)$$

where

$$E_1 = \frac{C_1}{1 + \kappa} \quad (56)$$

$$E_2 = \frac{C_2}{1 + \kappa} \quad (57)$$

$$Nu_{FD} = Nu_1 = \left\{ \frac{\varphi_t}{2} + \frac{[\psi^2 \omega^3 - 8(2\psi + 1)\omega] I_0^2(\omega) + 16(2\psi + 1) I_0(\omega) I_1(\omega) + 8\omega I_1^2(\omega)}{8\omega[\psi \omega I_0(\omega) - 2I_1(\omega)]^2} \right\}^{-1} \quad (63)$$

$$E_3 = -E_1 [I_0(\omega) + \varphi_t \omega I_1(\omega)] - E_2 (1 + 2\varphi_t) \quad (58)$$

Following the way done for  $\theta_{f,b}$  in the LTNE model, the dimensionless bulk mean fluid temperature  $\theta_{f,b1}$  in the LTE model becomes

$$\begin{aligned} \theta_{f,b1} &= 2 \int_0^1 \hat{u} \theta \eta \, d\eta \\ &= E_1 g_1 [I_0^2(\omega) - I_1^2(\omega)] + E_2 g_1 \frac{2}{\omega^2} \left[ \left( \omega + \frac{4}{\omega} \right) I_1(\omega) - 2I_0(\omega) \right] \\ &\quad + [E_1 g_2 + E_3 g_1] \frac{2}{\omega} I_1(\omega) + \frac{1}{2} (E_2 + 2E_3) g_2 \end{aligned} \quad (59)$$

Similarly, the average Nusselt number on the tube wall, based on the overall thermal conductivity,  $k_{eq}$ , is written as

$$Nu_1 = -\frac{2}{(1 + \kappa) \theta_{f,b1}} \quad (60)$$

Further, substituting Eqs. (32), (33) and (56)–(58) into Eq. (55) gives rise to the dimensionless temperature

$$\theta = \frac{1}{1 + \kappa} \frac{2\theta_{FD}}{Nu_{FD}} \quad (61)$$

where  $\theta_{FD}$  and  $Nu_{FD}$  are exactly the same as those obtained by Nield and Kuznetsov [6] and given by

$$\theta_{FD} = g_2 Nu_{FD} \left[ \frac{1}{4} (\eta^2 - 1) + \frac{I_0(\omega) - I_0(\omega\eta)}{\psi \omega^2 I_0(\omega)} \right] - \frac{\varphi_t}{2} Nu_{FD} \quad (62)$$

The wall temperature  $T_{w1}$ , the bulk mean temperature  $T_{f,b1}$  and their difference are respectively obtained as

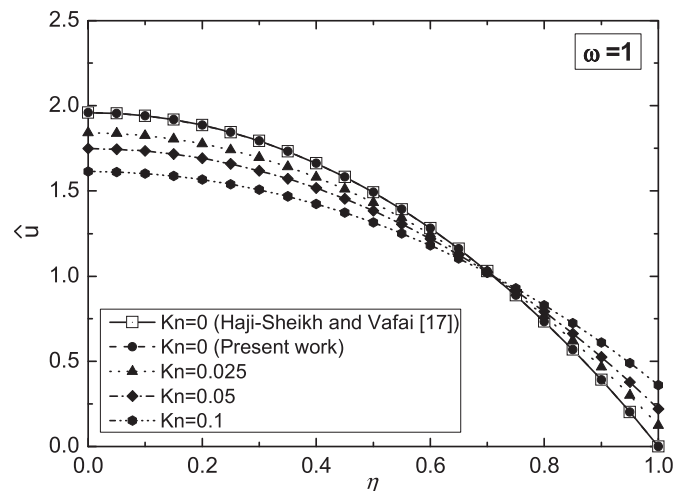


Fig. 2. Comparison of the present analytical dimensionless velocity distribution with that obtained by Haji-Sheikh and Vafai [17] and the effect of variations in the Knudsen number.

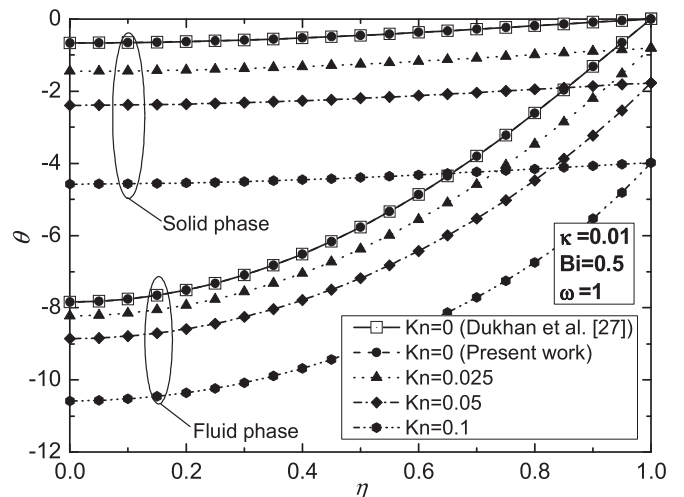


Fig. 3. Comparison of the present analytical dimensionless temperature distribution with that obtained by Dukhan et al. [26] and the effect of variations in the Knudsen number.

**Table 1**  
Comparison of the Nusselt number from the present analytical solution with that obtained by Nield and Kuznetsov [6] ( $\kappa = 1, Bi = 10, \omega = 1$ ).

$Kn$	LTNE (Eq. (42))				LTE	
	$Bi = 10$	$10^2$	$10^4$	$10^6$	Eq. (60)	Nield and Kuznetsov
0.0	2.939	4.194	4.413	4.415	4.415	4.415
0.001	2.932	4.186	4.404	4.407	4.406	4.406
0.002	2.924	4.178	4.396	4.398	4.398	4.398
0.004	2.909	4.159	4.378	4.380	4.380	4.380
0.006	2.894	4.139	4.360	4.362	4.362	4.362
0.008	2.878	4.119	4.341	4.343	4.344	4.344
0.01	2.861	4.099	4.321	4.324	4.324	4.324
0.02	2.768	3.986	4.219	4.224	4.224	4.224
0.04	2.561	3.733	3.998	4.007	4.008	4.008
0.06	2.349	3.469	3.770	3.785	3.787	3.787
0.08	2.148	3.213	3.548	3.569	3.571	3.571
0.1	1.965	3.213	3.338	3.364	3.367	3.367

$$T_{w1} = \frac{2q_w \varepsilon}{R\rho c_p u_e} z - \frac{q_w R}{k_{s,eff}} \theta_{f,b1} + T_e \tag{64}$$

$$T_{f,b1} = T_{f,b} = \frac{2q_w \varepsilon}{R\rho c_p u_e} z + T_e \tag{65}$$

$$T_{w1} - T_{f,b1} = -\frac{q_w R}{k_{s,eff}} \theta_{f,b1} \tag{66}$$

**4. Results and discussion**

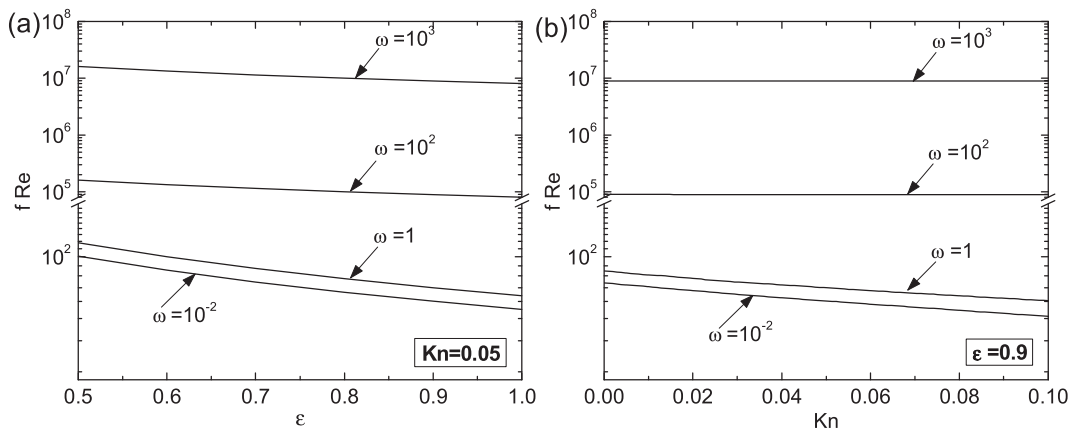
For all of the presented results, it is assumed that  $\gamma = 1.4$  and  $Pr = 0.707$  unless otherwise noted. First, the proposed exact solutions are validated by comparing some limiting results available in the literature. Fig. 2 depicts the dimensionless velocity distribution along the radial direction for no-slip flow regime ( $Kn = 0$ ) with  $\omega = 1$ . The results are in complete agreement with the analytical velocity distribution obtained by Haji-Sheikh and Vafai [17]. The case of the velocity slip is also displayed in Fig. 2 with Knudsen number  $Kn = 0.025, 0.05$  and  $0.1$ . It is obviously seen from the figure that as the value of  $Kn$  increases, the velocity slip at the wall increases. It is worth mentioning that the velocity gradient at the wall for the slip flow decreases as compared to the no-slip flow. This implies that higher  $Kn$  reduces the retarding effect of the wall and yields more flow passing through the microtube.

Fig. 3 depicts the dimensionless temperature distribution with  $\kappa = 0.01, Bi = 0.5$  and  $\omega = 1$ . The Knudsen number has been set to zero to compare our analytical solution with the work of Dukhan et al. [26]. An excellent agreement is observed between these solutions. Also, the temperature distributions for  $Kn = 0.025, 0.05$  and  $0.1$  are plotted in Fig. 3. As expected, the temperature profile shifts down with increasing  $Kn$ , but the normal temperature gradient of the tube wall remains constant due to the isoflux boundary condition. Centerline temperatures for both phases decrease with an increase in the Knudsen number.

We have also compared our results with those obtained by Nield and Kuznetsov [6] for the limiting case of  $Bi \rightarrow \infty$ . As seen from Table 1, an excellent agreement is found. Moreover, an increase in the Knudsen number renders a decrease in the Nusselt number. This is because of a decrease in heat transfer due to the rarefaction effects.

Fig. 4 illustrates the variation of  $fRe$  with the porosity or the Knudsen number at  $\omega = 10^{-2}, 1, 10^2$  and  $10^3$ . As seen from Fig. 4(a),  $fRe$  decreases with an increase in  $\varepsilon$ . An increase in the porosity results in a decrease in the volume fraction of solid matrix, which relieves the flow resistance and in turn reduces the wall friction. Fig. 4(b) demonstrates that  $fRe$  decreases as Knudsen number increases when  $\omega \leq 1$  while  $fRe$  remains almost independent of  $Kn$  when  $\omega \geq 10^2$ . It is known that an increase in Knudsen number would lead to an enhancement in  $Re$  due to the increase in the flow velocity and a reduction in  $f$  due to the gas rarefaction at the tube wall. For lower values of  $\omega$  the wall friction (Brinkman shear stress term) predominates in the competition with the Darcy viscous drag while for higher values of  $\omega$  their impacts on  $fRe$  are very close to each other.

The effect of the Biot number on the Nusselt number is shown in Fig. 5 for  $\kappa = 0.1$  and  $\omega = 0.1, 1, 10$  and  $10^2$ . As expected, an increase in  $Bi$  yields an increase in the Nusselt number. Increasing  $Bi$  translates to an enhancement in interstitial heat transfer. For large values of  $Bi$ , specifically for  $Bi > 10^3$ ,  $Nu$  tends to asymptotic values. As mentioned above, the LTNE model reduces to the LTE one as  $Bi \rightarrow \infty$ . Hence, these asymptotic values will converge to the LTE solutions as  $Bi$  increases. For a fixed value of  $Bi$ , the higher the Knudsen number, the lower the Nusselt number. Higher  $Kn$  implies fewer molecules collide with the heated wall and carry part of the energy at the wall. As a consequence, it increases the temperature difference between the wall and the bulk fluid, which is the main driving force for the heat transfer. It is worth commenting that the change in  $Nu$  is more severe when the value of  $Bi$  falls in the range between 1 and  $10^2$ . Also, this figure demonstrates that for lower porous media shape factors ( $\omega \leq 1$ ), the Nusselt number is less



**Fig. 4.** Effect of (a) the porosity and (b) Knudsen number on the Fanning friction factor.

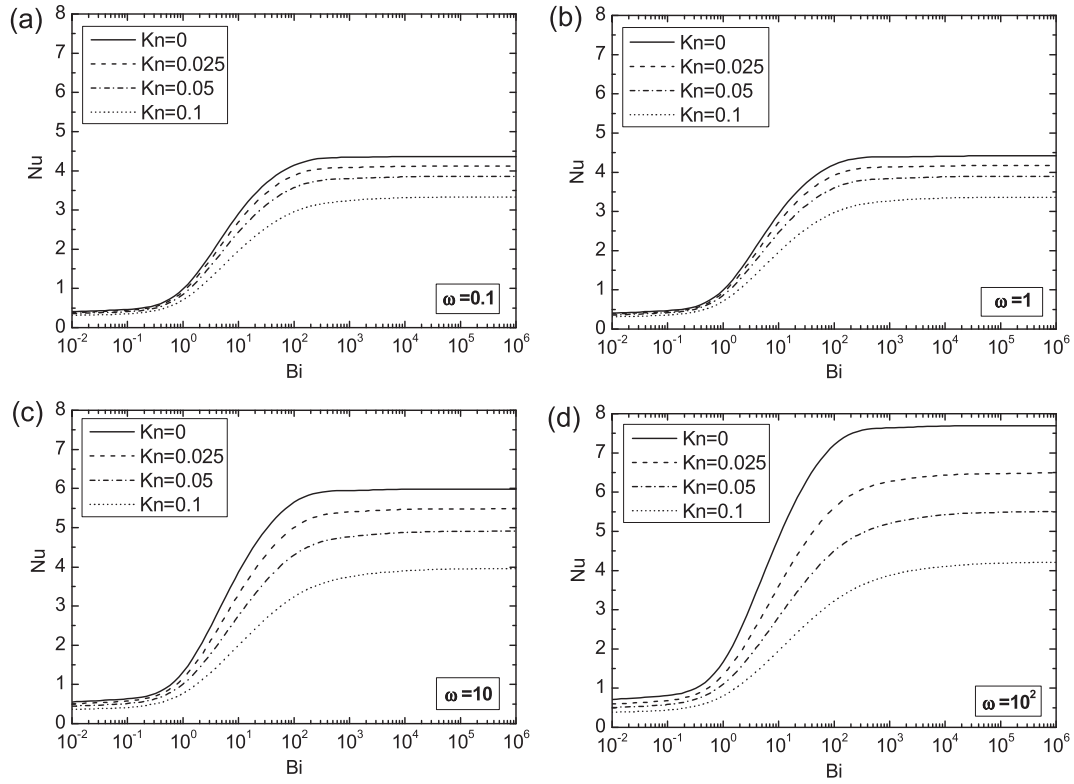


Fig. 5. Effect of Knudsen and Biot numbers on the Nusselt number at different porous media shape factors for  $\kappa = 0.1$ : (a)  $\omega = 0.1$ , (b)  $\omega = 1$ , (c)  $\omega = 10$  and (d)  $\omega = 10^2$ .

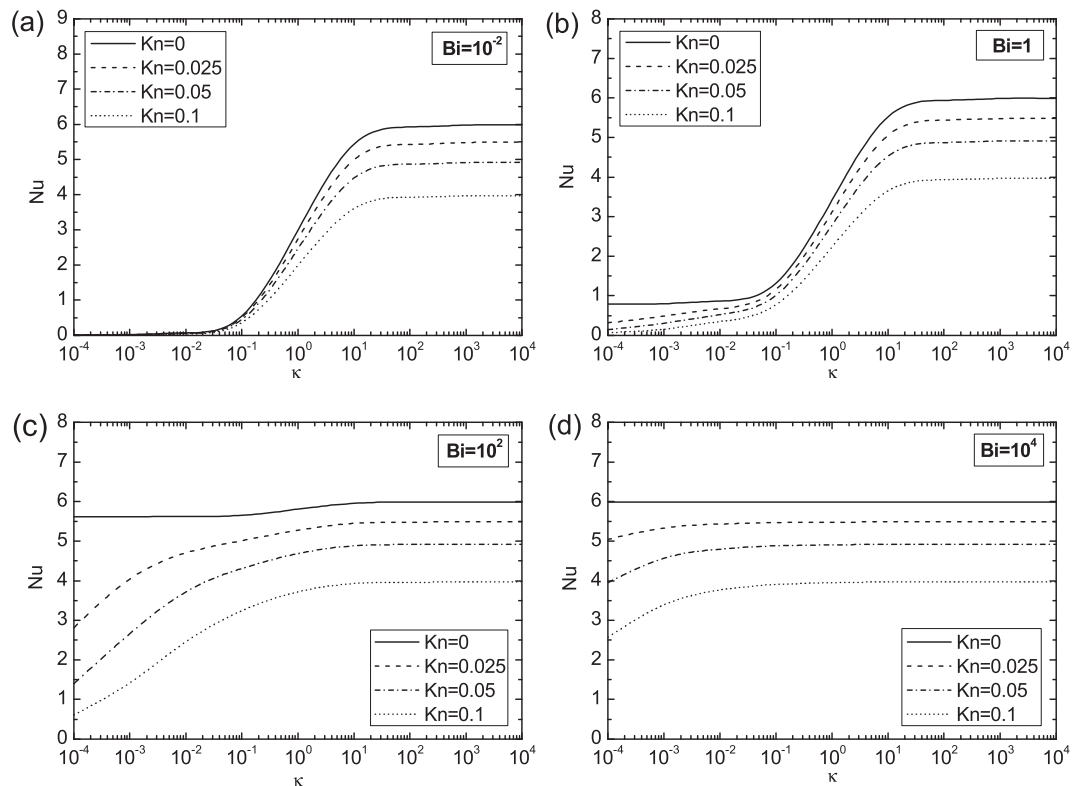


Fig. 6. Effect of Knudsen number and the effective thermal conductivity ratio on the Nusselt number at different Biot numbers for  $\omega = 10$ : (a)  $Bi = 10^{-2}$ , (b)  $Bi = 1$ , (c)  $Bi = 10^2$  and (d)  $Bi = 10^4$ .

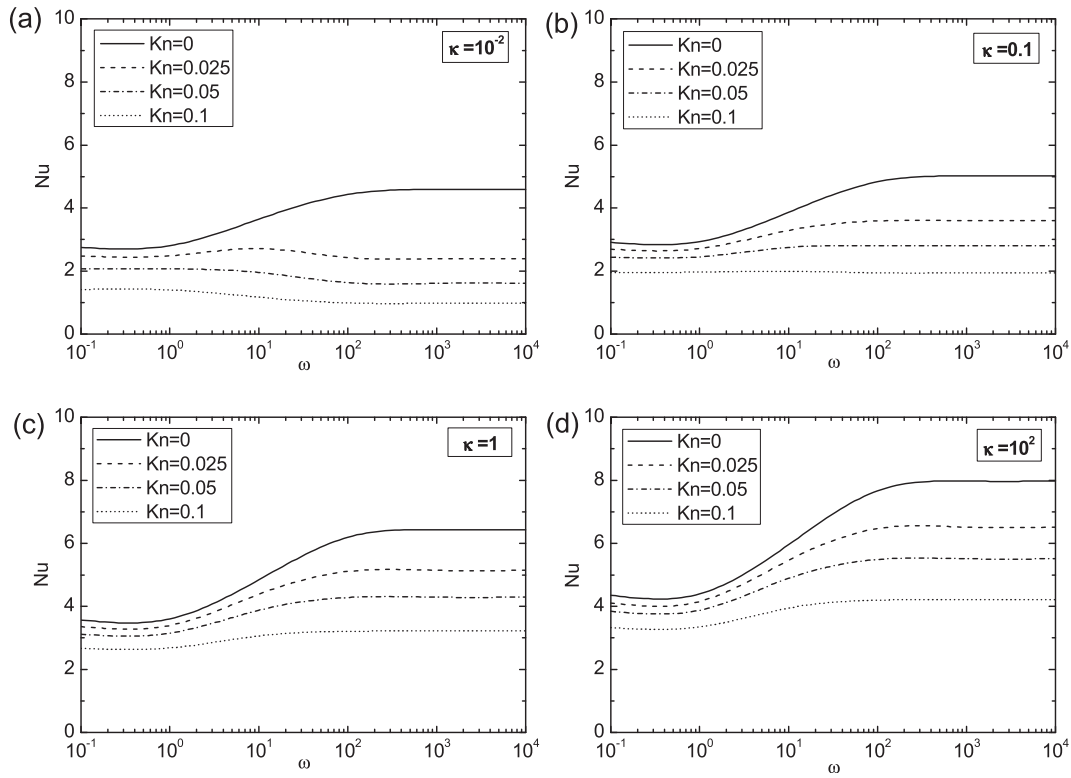


Fig. 7. Effect of Knudsen number and the porous media shape factor on the Nusselt number at different thermal conductivity ratios for  $Bi = 10$ : (a)  $\kappa = 10^{-2}$ , (b)  $\kappa = 0.1$ , (c)  $\kappa = 1$  and (d)  $\kappa = 10^2$ .

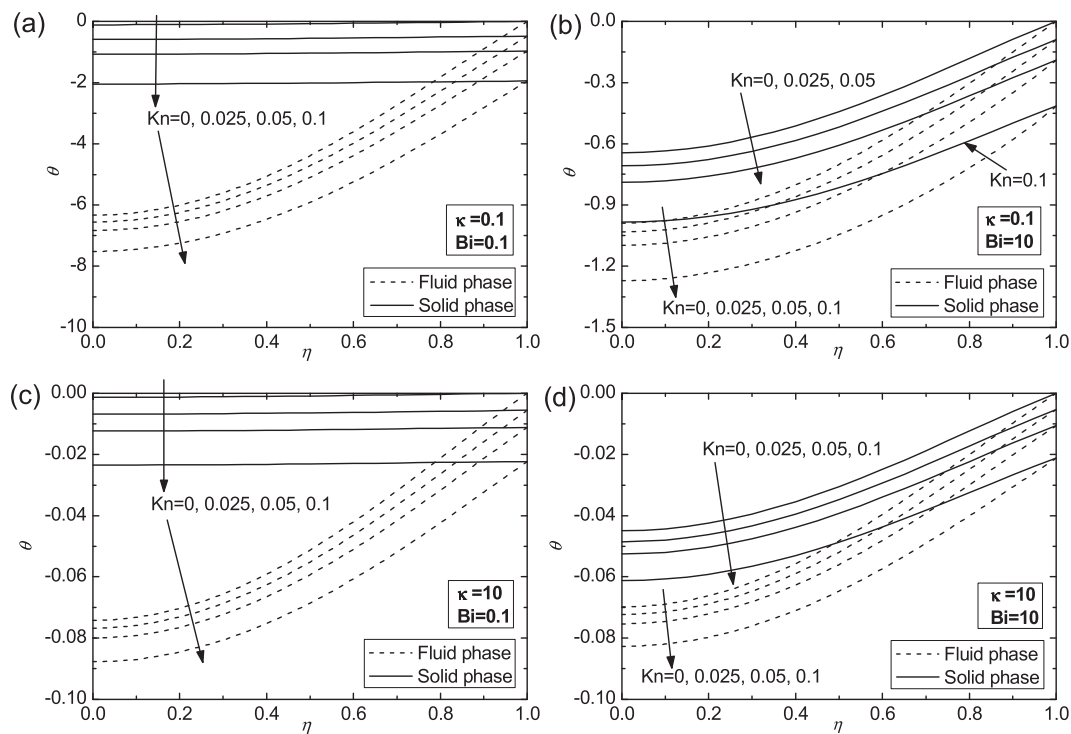


Fig. 8. Effect of Knudsen number on the dimensionless temperature distribution along the radial direction for  $\omega = 1$ : (a)  $\kappa = 0.1, Bi = 0.1$ , (b)  $\kappa = 0.1, Bi = 10$ , (c)  $\kappa = 10, Bi = 0.1$  and (d)  $\kappa = 10, Bi = 10$ .

**Table 2**

Nusselt number for air and helium at the microtube wall subject to a constant heat flux ( $\kappa = 0.1$ ,  $Bi = 10$ ,  $\omega = 1$ ).

$\sigma_v$	$\sigma_t$	$Kn = 0.001$	0.01	0.02	0.04	0.06	0.08	0.1
<i>Air</i> ( $Pr = 0.707$ , $\gamma = 1.4$ )								
0.95	0.95	2.933	2.876	2.803	2.638	2.464	2.293	2.131
	0.85	2.930	2.848	2.749	2.540	2.333	2.138	1.962
	0.75	2.927	2.814	2.684	2.425	2.185	1.970	1.782
0.85	0.95	2.934	2.889	2.823	2.663	2.485	2.308	2.140
	0.85	2.932	2.861	2.768	2.561	2.349	2.148	1.965
	0.75	2.928	2.826	2.701	2.442	2.195	1.974	1.780
0.75	0.95	2.936	2.905	2.848	2.691	2.509	2.325	2.149
	0.85	2.934	2.876	2.791	2.585	2.366	2.157	1.968
	0.75	2.930	2.840	2.722	2.462	2.207	1.977	1.777
<i>Helium</i> ( $Pr = 0.68$ , $\gamma = 1.667$ )								
0.95	0.60	2.916	2.716	2.507	2.139	1.838	1.596	1.400
	0.45	2.912	2.596	2.305	1.849	1.518	1.274	1.090
	0.30	2.874	2.386	1.985	1.454	1.126	0.900	0.756
0.925	0.60	2.916	2.719	2.510	2.141	1.838	1.594	1.398
	0.45	2.902	2.598	2.307	1.849	1.517	1.272	1.087
	0.30	2.875	2.388	1.986	1.453	1.124	0.906	0.753
0.90	0.60	2.917	2.721	2.513	2.143	1.838	1.593	1.395
	0.45	2.903	2.601	2.309	1.849	1.516	1.270	1.084
	0.30	2.875	2.389	1.987	1.452	1.122	0.903	0.750

sensitive to the rarefaction effects. As expected, for  $\omega > 10^2$ , the heat transfer is strongly dependent on the rarefaction. The values of  $Nu$  are bounded between 4.36 (plane Poiseuille flow,  $\omega \rightarrow 0$ ) and 8 (slug flow,  $\omega \rightarrow \infty$ ). This is in accordance with the conclusions of Hooman and Ranjbar-Kani [27].

Fig. 6 depicts the impact of the effective thermal conductivity ratio on the Nusselt number for  $\omega = 10$  and  $Bi = 10^{-2}$ ,  $1$ ,  $10^2$  and  $10^4$ . A larger effective thermal conductivity ratio physically implies an enhancement in the contribution of forced convection currents. As expected, increasing  $\kappa$  leads to an increase in  $Nu$ . It is seen that the asymptotic values of  $Nu$  appear when  $\kappa > 10^2$ . As shown in Fig. 6(d),  $Nu$  does not strongly depend on  $\kappa$  for higher values of  $Bi$ . This is due to the fact that the behavior of the LTNE model approaches that of the LTE model where  $Nu$  is independent of  $\kappa$  according to Eq. (60) or Eq. (63).

Fig. 7 displays the variation of Nusselt number with the porous media shape factor for  $Bi = 10$ . It can be seen that as  $\omega$  increases, first,  $Nu$  decreases slightly, then it increases and finally approaches its asymptotic value. Lower  $\omega$  values ( $\omega < 1$ ) are related to higher Darcy numbers and greater permeability while larger  $\omega$  values ( $\omega > 500$ ) are associated with smaller Darcy numbers and lower permeability. As discussed before, the rarefaction decreases the heat transfer, i.e. increasing  $Kn$  leads to a reduction in  $Nu$ .

Fig. 8 delineates the effect of Knudsen number on the temperature distribution with various combinations of the effective thermal conductivity ratio and Biot numbers. As expected, increasing  $Bi$  renders a reduction in the temperature difference between the fluid and solid phases. However, the influence of  $\kappa$  on the temperature difference is not remarkable. As illustrated, increasing  $Kn$  gives rise to an increase in the temperature jump at the wall. This is due to the reduction in the interaction between the gas molecules and the heated wall. As  $Kn$  increases, the mean free path length of the gas molecules increases and any molecule reflected from the wall has less opportunity to collide with other molecules. The increase in the temperature jump reduces the energy transmission from the heated wall to the gas.

Table 2 displays the rarefaction effects for air and helium based on various combinations of  $\sigma_v$ ,  $\sigma_t$  and  $Kn$ . Obviously, an enhancement in  $Nu$  is observed as  $\sigma_t$  increases for an assigned value of  $\sigma_v$ .

## 5. Conclusions

Slip-flow and heat transfer in a porous circular microtube is investigated analytically under the constant heat flux and LTNE conditions. The flow through the porous microtube is described by the Brinkman-extended Darcy flow model. Exact solutions for fully developed velocity and temperature distributions as well as the average Nusselt number are derived incorporating rarefaction effects at the tube wall. Compared to the no-slip flow regime ( $Kn = 0$ ), the slip-flow counterpart ( $10^{-3} < Kn \leq 10^{-1}$ ) is associated with a reduction in wall friction (for lower values of  $\omega$ ) and an increase in the temperature difference between the wall and the bulk fluid, resulting in a decrease in the heat transfer. Furthermore, as  $\omega \rightarrow 0$  the Brinkman flow reduces to the Poiseuille flow, hence the present analytical solutions are applicable for the clear fluid case. Our analytical results can be extended to handle more complicated microchannels with multiply connected cross sections such as coaxial cylindrical annuluses.

## Acknowledgments

This work was supported by the Visiting Scholar Program for Young Faculty in Shanghai, China. The authors would like to acknowledge this support.

## References

- [1] Z.P. Duan, Y.S. Muzychka, Slip flow heat transfer in annular microchannels with constant heat flux, *J. Heat Transfer* 130 (2008) 092401.1–092401.8.
- [2] F.E. Larrode, C. Housiadas, Y. Drossinos, Slip-flow heat transfer in circular tubes, *Int. J. Heat Mass Transfer* 43 (2000) 2669–2680.
- [3] M. Renksizbulut, H. Niazmand, G. Tercan, Slip-flow and heat transfer in rectangular microchannels with constant wall temperature, *Int. J. Therm. Sci.* 77 (2014) 870–881.
- [4] H. Bahrami, T.L. Bergman, A. Faghri, Forced convective heat transfer in a microtube including rarefaction, viscous dissipation and axial conduction effects, *Int. J. Heat Mass Transfer* 5 (2012) 6665–6675.
- [5] B. Buonomo, O. Manca, G. Lauriat, Forced convection in micro-channels filled with porous media in local thermal non-equilibrium conditions, *Int. J. Therm. Sci.* 77 (2014) 206–222.
- [6] D.A. Nield, A.V. Kuznetsov, Forced convection with slip-flow in a channel or duct occupied by a hyper-porous medium saturated by a rarefied gas, *Transp. Porous Media* 64 (2006) 161–170.
- [7] A.V. Kuznetsov, D.A. Nield, Thermally developing forced convection in a porous medium occupied by a rarefied gas: parallel plate channel or circular tube with walls at constant heat flux, *Transp. Porous Media* 76 (2009) 345–362.
- [8] O.M. Haddad, M.A. Al-Nimr, M.S. Sari, Forced convection gaseous slip flow in circular porous micro-channels, *Transp. Porous Media* 70 (2007) 167–179.
- [9] K. Hooman, Slip flow forced convection in a microporous duct of rectangular cross-section, *Appl. Therm. Eng.* 29 (2009) 1012–1019.
- [10] H. Shokouhmand, A.H. Meghdadi Isfahani, E. Shirani, Friction and heat transfer coefficient in micro and nano channels with porous media for wide range of Knudsen number, *Int. Commun. Heat Mass Transfer* 37 (2010) 890–894.
- [11] S.M.H. Hashemi, S.A. Fazeli, H. Shokouhmand, Fully developed non-Darcian forced convection slip-flow in a micro-annulus filled with a porous medium: analytical solution, *Energy Convers. Manag.* 52 (2011) 1054–1060.
- [12] O.M. Haddad, M.A. Al-Nimr, Y. Taamneh, Hydrodynamic and thermal behavior of gas flow in microchannels filled with porous media, *J. Porous Media* 9 (2006) 403–414.
- [13] K. Hooman, Heat and fluid flow in a rectangular microchannel filled with a porous medium, *Int. J. Heat Mass Transfer* 51 (2008) 5804–5810.
- [14] D.S. Chauhan, V. Kumar, Effects of slip conditions on forced convection and entropy generation in a circular channel occupied by a highly porous medium: Darcy extended Brinkman–Forchheimer model, *Turk. J. Eng. Environ. Sci.* 33 (2009) 91–104.
- [15] W.J. Minkowycz, A. Haji-Sheikh, K. Vafai, On departure from local thermal equilibrium in porous media due to a rapidly changing heat source: the Sparrow number, *Int. J. Heat Mass Transfer* 42 (1999) 3373–3385.
- [16] O.M. Haddad, M.A. Al-Nimr, J. Sh. Al-Omary, Forced convection of gaseous slip flow in porous micro-channels under local thermal non-equilibrium conditions, *Transp. Porous Media* 67 (2007) 453–471.
- [17] A. Haji-Sheikh, K. Vafai, Analysis of flow and heat transfer in porous media imbedded inside various-shaped ducts, *Int. J. Heat Mass Transfer* 47 (2004) 1889–1905.

- [18] A. Amiri, K. Vafai, Analysis of dispersion effects and non-thermal equilibrium non-Darcian, variable porosity incompressible flow through porous medium, *Int. J. Heat Mass Transfer* 27 (1994) 939–954.
- [19] E.H. Kennard, *Kinetic Theory of Gases*, McGraw-Hill, New York, 1939.
- [20] S. Chapman, T.G. Cowling, *The Mathematical Theory of Non-uniform Gases*, third ed., Cambridge University Press, London, 1970.
- [21] C. Cai, Q. Sun, I.D. Boyd, Gas flows in microchannels and microtubes, *J. Fluid Mech.* 589 (2007) 305–314.
- [22] K. Yang, K. Vafai, Analysis of temperature gradient bifurcation in porous media – an exact solution, *Int. J. Heat Mass Transfer* 53 (2010) 4316–4325.
- [23] D.Y. Lee, K. Vafai, Analytical characterization and conceptual assessment of solid and fluid temperature differentials in porous media, *Int. J. Heat Mass Transfer* 42 (1999) 423–435.
- [24] W. Lu, C.Y. Zhao, S.A. Tassou, Thermal analysis on metal-foam filled heat exchangers – part 1. Metal foam filled pipes, *Int. J. Heat Mass Transfer* 49 (2006) 2751–2761.
- [25] S. Mahjoob, K. Vafai, Analytical characterization of heat transfer through biological media incorporating hyperthermia treatment, *Int. J. Heat Mass Transfer* 52 (2009) 1608–1618.
- [26] N. Dukhan, M.A. Al-Rammahi, A.S. Suleiman, Fluid temperature measurements inside metal foam and comparison to Brinkman–Darcy flow convection analysis, *Int. J. Heat Mass Transfer* 67 (2013) 877–884.
- [27] K. Hooman, A.A. Ranjbar-Kani, A perturbation based analysis to investigate forced convection in a porous saturated tube, *J. Comput. Appl. Math.* 162 (2004) 411–419.